International Journal of Nanoelectronics and Materials

In Press, Accepted Manuscript – Note to user

Optical, Electrical and Photovoltaic Studies of γ-MnS Thin Films Deposited by Spray Pyrolysis Technique

Z. AMARA, M. KHADRAOUI, R. MILOUA

Laboratoire d'Elaboration et de Caractérisation des Matériaux (LECM), département d'électronique, Université Djillali Liabes, BP89, Sidi Bel Abbés 22000.Algérie

ABSTRACT

γ-MnS thin films were prepared on glass substrate by spray pyrolysis method at 280 °C. The optical constants and thickness of the films were extracted using the pattern search optimization technique in combination with a seed preprocessing procedure (spPS). Refractive index dispersion of the films was analyzed by using the concept of the single oscillator model. The values of the oscillator energy, $E_{0,}$ and the dispersion energy, $E_{d,}$ were determined as 8.83 eV and 5.65 eV, respectively. The analysis of the optical properties of the γ-MnS film showed a direct transition with energy band gap of 2.74 eV. Utilizing Hall Effect measurement, we have determined values of the resistivity ρ which equals to 1150 Ωcm. The positive value of hall coefficient showed a p-type in nature of the obtained thin film. The maximum of photocurrent density estimated by Yablonovitch limit is equal to 46 mA/cm^2.

Keywords:

γ-MnS, Thin film, optical properties, Single-oscillator model, Hall Effect measurement.

1. Introduction.

In the last few decades, manganese chalcogenides MnX (X = O; S; Se; Te) have been paid a great attention by many researchers due to their interesting electronic structure and magneto-optical properties **[1-4].** Manganese sulfide that belongs to VII-VI group is known as a diluted

magnetic semiconductor DMS **[5,6]** and a wide gap (E_g = 3.1 eV) , which can be used as a window/buffer material in solar cell **[7].** MnS is known to crystallize into three forms*:* the rock salt α-MnS and the two others β-MnS together with γ-MnS.

Furthermore, several reports are available in several literatures for the preparation and the characterization of MnS thin films. The production of these films has been carried out by various physical and chemical deposition techniques such as chemical bath deposition **[8-9-10]**, MBE **[11],** microwave hydrothermal **[12],** solvothermal**[13],** thermal vaccum evaporation**[14]** and spray pyrolysis **[5,6]**,**[15-17].** Recently, among these methods, spray pyrolysis has gained a most attention because it is an economic and simple technique to obtain a homogeneous and adherent thin film.

Mahindra et al **[18]** studied the effect of biofield energy treatment on the atomic and physical properties of MnS films. Shi et al had also studied the effect of Boric Acid content on the structural and optical properties of MnS. Girish et al **[19]** discussed the effect of the concentration of the solution with EDTA on the physical properties. Gui et al **[20]** is observed the effect of temperature, pH and time on the phase and morphologies of MnS nanocrystals.

The key point of this work is to determine both the crystallite size and the microstrain by using Willimson-Hall plot. The compositional details were analyzed using scanning electron microscopy (SEM) and energy dispersive analysis of X-ray (EDAX) analyzer. Furthermore, the pattern search technique in combination with a seed preprocessing procedure (spSP) technique has been used to determine the optical constants (n, k, ε_1, ε2) of γ-MnS thin film. The analysis of the optical refractive index n was conducted by single oscillator model proposed by Wemple and DiDomenico to determine the dispersion energy parameters. Likewise, the Hall Effect measurement of the obtained thin films was carried out to determine the resistivity, mobility, hall coefficient, and carrier concentration. The deposited thin films yield a photocurrent of 46 mA/cm^2 at an equivalent thickness of 1 μm, using yablonovitch limit configuration.

2. Experimental details.

γ-MnS thin films have been deposited at substrate temperature of 280 °C by Spray pyrolysis technique. The starting chemical solution was prepared using 0.1 M of $MnCl_2.4H_2O$ and Thiourea ($CS(NH_2)_2$). The prepared solutions of manganese chloride and thiourea were appropriately mixed to obtain Mn:S proportion of 1:3. The obtained solution was pulverised

on glass substrates with compressed air (2 bars) and at flow rate of 8ml/min. The distance from the spray nozzle to the heater is kept approximately at 27 cm (see **Fig. 1**). Under these deposition conditions, good films were obtained with smooth surfaces and adherent to the substrates. Structural characterization has been carried out at room temperature using a Bruker diffractometer with Cu-Kα radiation (λ = 1.5405Å). The optical transmittance and reflectance was recorded from 200 to 2500 nm wavelength using an UV (Ultra-Violet) Visible JASCO type V-570 double beam spectrophotometer. The composition and the surface morphology of the deposited thin films were determined by JEOL-JSM 5800 scanning electron microscope. Hall Effect measurements of the film were carried out using HMS-5000 system.

3. Results and discussion.

Crystallographic structure:

Fig.2 demonstrates the X-ray diffraction pattern of nanocystalline γ-MnS thin film deposited on glass substrates according to the experimental conditions mentioned previously. All peaks were indexed in according the experimental ASTM X-ray powder data files (Card No. 40-1289). The crystalline structure of γ-MnS was hexagonal and the parameters lattice was found a = 5.98Å; c = 6.25Å which are in good agreement with their values of JCPDS card.

The Williamson-Hall plot is used to estimate both crystallite size D and microstrain ε **[21]**. As we can see in **Fig. 3**, the linear fit of ($\frac{\beta cos\theta}{\lambda}$) versus($\frac{4sin\theta}{\lambda}$) curve gives values of microstrain from the slope and the crystallite size from the intercept which are D = 62.8 nm and ε = 1.4310^{-3}.

EDS and SEM analyses:

The obtained EDX results show that it is often necessery to identify the different elements associated with the sample. **Fig. 4** depicts the EDX spectrum. It is clearly shown that no other impurities is present in the film. There is an impoverishment in sulfur. This must be due to its evaporation with temperature. The number of X-Ray line (K) that an element can emit is dependent on the atomic number (Z) and the acceleration tension. The qualitative analysis identifies the present elements in the sample; here we have only the Mn and S. In addition, the quantitative analysis specifies the amount of chemical content. **Table.1** represents the EDX results of γ-MnS thin film. Furthermore, **Fig. 5** depicts SEM images of γ-MnS thin film

deposited on glass substrate. It is clear that the film obtained is dense, adherent, and homogeneous in surface morphology and coats the totality of glass substrate.

Optical studies:

The inter-band absorption theory shows that the absorption coefficient near the threshold versus the energy adheres to the following relation **[22]**

$$(\alpha h\omega) = A_n(h\omega - E_g)^n \quad (1)$$

where A_n is the probability parameter for the transition and E_g the optical gap energy. For allowed direct transitions the coefficient n is equal to ½ and for indirect allowed transitions n = 2. The plot of $(\alpha h\omega)^2$ versus energy is shown in **Fig. 6**. The nature of the plot indicates the existence of direct transitions. The bandgap E_g is determined by extrapolation of the straight portion of the plot to the energy axis which corresponds to the direct band-gap transition of the γ-MnS was equal to 2.74 eV.

The optical constants of γ-MnS thin films:

The study of the optical constants n, k, ε_1, ε_2 gives information to the optical behavior of a material. These constants are calculated by spPS (seed processing Pattern Search) technique **[23]**. The variation of n and k with wavelength λ is represented in **Fig. 7**. As can be seen in this figure, the refractive index n was varied between 1.55 and 1.7 in the meantime [300nm-1000nm]**.** It is high in the NIR range. Also, it is noted that the extinction coefficient k is in order of 0.35 in the region (250nm-500nm). It's dependent with the absorption coefficient α.

The real and the imaginary parts (ε_1 & ε_2) of the dielectric constant ε are illustrated in the same **Fig. 7**, where ε_1 varies in a growing way between 2.4 to 2.85 in the region 300nm-750nm and ε_2 is in order 1.2 in the range 250nm-500nm, they follow the same behavior of n and k respectively. Using the spPS technique, we have estimated the film thickness equals 303 nm.

Dispersion behavior of refractive index :

The refractive index n is found to decrease with increment of wavelength, and tends to be constant at higher values of wavelength. At low wavelength values, the refractive index presents a normal dispersion. Beyond this region, the thin film becomes non diepersive. The dispersion parameters of different materials (crystalline and non crystalline) were evaluated by the single oscillator model of the refractive index n below the interband absorption edge **[24]**. This model is proposed by Wemple and DiDomenico, which is given as follows **[25]**

$$n^2 = 1 + \frac{E_0 E_d}{E_0^2 - (h\upsilon)^2} \quad (2)$$

where n is refractive index, E_0 is the energy of effective dispersion oscillator, (hυ) is the photon energy and E_d is the dispersion energy. E_0 and E_d have a significant association with the crystalline structure and iconicity of ionic or covalent materials. $(n^2-1)^{-1}$ against $(h\upsilon)^2$ plot of γ-MnS thin film is represented in **Fig. 8.** The E_0 and E_d was determined from the slope $(E_0E_d)^{-1}$ and the intercept ($\frac{E0}{Ed}$) on the vertical axis of the linear fit of $(n^2-1)^{-1}$ vs $(h\upsilon)^2$.

The M_{-1} and M_{-3} moments can be extracted from the following relations **[26]**

$$E_0^2 = \frac{M_{-1}}{M_{-3}}; \quad E_d^2 = \frac{M_{-1}^3}{M_{-3}} \quad (3)$$

The values of E_0, Ed, M_{-1} and M_{-3} are summarized in **Table. 1.** The refractive index dependence on wavelengths is given by the following expression: **[27]**

$$\frac{n_\infty^2 - 1}{(n^2-1)} = 1 - \left(\frac{\lambda_0}{\lambda}\right)^2 \quad (4)$$

Fig. 9 shows plot of $(n^2-1)^{-1}$ vs $(\lambda)^{-2}$ whereby the linear fitting of this curve gives the values of n_∞ and λ_0 from the slope and the intercept. The value of $(n_\infty)^2$ at λ_0 was equal to high frequency dielectric constant ε_∞. These values are represented in **Table. 3.** As we can see**,** the variation between ε_∞ and ε_L is probably due to the free carrier contribution

The analyses of the refractive index n helps to give the lattice high frequency dielectric constant ε_L and $(\frac{N}{m^*})$ ratio by plotting n^2 versus λ^2 from **Fig. 10,** using the relationship below **[28]**

$$n^2 = \varepsilon_L - \left(\frac{e^2}{4\pi c^2}\frac{N}{m^*}\right)\lambda^2 \quad (5)$$

where ε_L and $\left(\frac{N}{m^*}\right)$ ratio are estimated from the slope and the intercept respectively of the linear fit of (n^2) vs (λ^2) plot. Values of ε_L and $\left(\frac{N}{m^*}\right)$ are represented in **Table. 2.**

Electrical study:

In order to determine the electrical properties of γ-MnS thin film such as resistivity ρ, mobility μ, carrier concentration n…, we have used Hall Effect measurement. The results are summarized in **Table. 4**. The positive value of hall coefficient indicates that the films are p-type in nature.

Photovoltaic study:

Using the measured absorption coefficient $\alpha(\lambda)$, we estimate the expected absorption capacity and photocurrent of the films. We assumed γ-MnS based solar cell with Yablonovitch limit configuration **[29].** It represents the maximum of light absorbed by films with fewer optical losses and evaluates the efficiency of light trapping which is calculated by the following equation [**29]**

$$A(d)_{\text{Yablonovitch}} = 1 - \frac{1}{1+\alpha d 4n^2} \quad (5)$$

where d is the film thickness, n is the refractive index and α is the absorption coefficient.

The thickness-dependent absorbed photon fraction and the photocurrent is calculated as follows **[30]**

$$Absorbed\ photon\ fraction = \frac{\int_{300\,nm}^{\lambda g} F(\lambda)A(d)\,d\lambda}{\int_{300\,nm}^{\lambda g} F(\lambda)\,d\lambda} \quad (6)$$

$$J_{ph}(d) = q \times \int_{300\,nm}^{\lambda g} F(\lambda)A(d)\,d\lambda \quad (7)$$

where $F(\lambda)$ is the AM1.5G photon flux, q is the electron charge and the wavelength $\lambda_g = hc/E_g$.

Fig. 11 shows the absorption versus films thickness. We notice that the maximum of absorption of γ-MnS thin films given by Yablonovitch limit is of 90%. On the other hand, the photocurrent is increased with the film thickness reaching a maximum of 46 mA/cm^2. Beyond this value, the short circuit current density became constant which is depicted in **Fig. 12.**

4. Conclusion.

Nanocrystalline γ-MnS thin film was prepared on glass substrates by spray pyrolysis technique at 280 °C. The surface morphology of γ-MnS thin film is dense and adherent and presents a good crystallinity of films. The pattern search optimization technique was successfully applied to extract the thickness and optical constants. The value of dispersion energy E_d determined by single-oscillator model was found to be 8.83 eV. The direct optical gap value corresponds to 2.74 eV. The values of resistivity ρ, mobility μ, carrier concentration n and Hall coefficient were also determined. Using the refractive index and the absorption coefficient values, we theoretically estimated the maximum of photocurrent density by Yablonovitch limit, which was equal to 46 mA/cm^2.

References

[1] S. Lei, K. Tang, Q. Yang, H. Zheng, Eur.J.Inorg.Chem. 20(2005)4124.

[2] Y. Zheng, Y. Cheng, Y. Wang, L. Zhou, F. Bao, C. Jia, J.Phys.Chem.B110(2006)8284.

[3] D. Fan, H. Wang, Y. Zhang, J. Cheng, B. Wang, H. Yan, Surf.Rev.Lett.11(2004)27e31.

[4] G. Pandey, H.K. Sharma, S.K. Srivastava, R.K. Srivastava, R.K. Kotnala, Mater. Res. Bull. 46(2011)1804e180.

[5] Lilac Amirav and Efrat Lifshitz, ChemPhysChem 2015, 16,353–359.

[6] M. Bedir, M. Özta, S.S. Çelika andT. Özdemir, ACTA PHYSICA POLONICA A. Vol. 126 (2014).

[7] M.N. Nnabuchi, Ph.D, The Pacific Journal of Science and Technology. Volume 7. Number 1. May 2006 (Spring).

[8] Sunil H. Chaki, Sanjaysinh, M. Chauhana, Jiten P. Tailorb, Milind, P. Deshpande. http://dx.doi.org/10.1016/j.jmrt.2016.05.003.

[9] YongShi, FanghongXue, ChunyanLi, QidongZhao, ZhenpingQu. Materials Research Bulletin 46(2011)483–486.

[10] Cemal Ulutas and Cebrail Gumus. American Institute of Physics. 080008 (2016).

[11] L. David, X. Tang, G. Beamson, D. Wolverson, K. A. Prior, and B. C. Cavenett. phys. stat. sol. (b) 241, No. 3, 471–474 (2004).

[12] XinYu, CaoLi-yun, HuangJian-feng, LiuJia, FeiJie, YaoChun-yan. Journal of Alloys and Compounds 549(2013)1–5.

[13] Yang Ren, Lian Gao, Jing Sun, Yangqiao Liu, Xiaofeng Xie. Ceramics International 38 (2012) 875–881.

[14] Amira Hannachi, Alfredo Segura, Hager Maghraoui-Meherzi. Materials Chemistry and Physicsxxx(2016)1-7

[15] Ahmet Yilmaz. Phys.Scr. 83 (2011)045603(5pp).

[16] M. R. I. Chowdhury, J. Podder, and A. B. M. O. Islam. Cryst. Res. Technol. 46, No. 3, 267 – 271 (2011).

[17] M. Girish, R. Sivakumar and C.Sanjeeviraja. Light and Its Interactions with Matter. 1620, 235-239 (2014).

[18] Mahendra Kumar Trivedi, Rama Mohan Tallapragada, Alice Branton, Dahryn Trivedi, Gopal Nayak, Omprakash Latiyal, Snehasis Jana. American Journal of Physics and Applications. 3(6): 215-220, 2015.

[19] M. Girisha, R. Sivakumarb, C. Sanjeevirajac, Y. Kuroki. Optik http: // dx.doi.org/10 .1016 /j.ijleo .2015.05.072.

[20] Yicai Gui, Liwu Qian, Xuefeng Qian. Materials Chemistry and Physics 125 (2011) 698–703.

[21] G. K. Williamson, W. H. Hall: Acta Metall., 1953, vol. 1, pp. 22.

[22] J. TAUC, A. MENTH. JOURNAL OF NON-CRYSTALLINE SOLIDS 8--10 (1972) 569-585.

[23] R. Miloua, Z. Kebbab, F. Chiker, K. Sahraoui, M. Khadraoui, N. Benramdane, Opt. Lett. 37 (2012) 4.

[24] F. YAKUPHANOGLU, S. ILICANb, M. CAGLARb, Y. CAGLAR. JOURNAL OF OPTOELECTRON CS AND ADVANCED MATER ALS Vol. 9, No. 7, July 2007, p. 2180 – 2185.

[25] S. H. Wemple and M. DiDomenico, Jr. PHYSICAL REVIEW B VOLUME 3, NUMB ER 4 15 F EBRUARY 1971.

[26] M.N. Amroun, M. Khadraoui, R. Miloua, Z. Kebbab, K. Sahraoui. Optik 131 (2017) 152–164.

[27] MujdatCaglar, SalihaIlican, YaseminCaglar, Y¨ ucelS¸ ahin, FahrettinYakuphanoglu , DenizH¨ ur. Spectrochimica Acta Part A 71(2008)621–627.

[28] M.M. EL-Nahass, A.A.M. Farag, E.M. Ibrahim et al, Vacuum 72 (2004) 453-460.

[29] Ken Xingze Wang, Zongfu Yu, Victor Liu, YiCui, and Shanhui Fan. dx. doi. Org 10. 1021/nl204550q | NanoLett. 2012,12,1616−1619.

[30] M. Khadraoui, R. Miloua, N. Benramdane, A. Bouzidi, K. Sahraoui. Materials Chemistry and Physics xxx (2015)1-7.

Figure captions:

Fig.1. Schematic diagram of the spraying pyrolysis process: (1) Aspiration system (2) spraying solution (3) carrier gas (4) glass substrates (5) thermocouple (6) hot plate.

Fig. 2. XRD patterns of γ-MnS thin film.

Fig. 3. Williamson-Hall plot of γ-MnS thin film.

Fig. 4. EDX analysis of γ-MnS thin film

Fig. 5. SEM image of γ-MnS thin film.

Fig. 6. $(\alpha h\upsilon)^2$ versus energy of γ-MnS thin films.

Fig. 7. Optical constants (n, k, ε_1, ε_2 versus energy wavelength of γ-MnS thin films.

Fig. 8. n^2 versus λ^2 of of γ-MnS thin films.

Fig. 9. $(n^2 - 1)$ versus $(h\upsilon)^2$ of γ-MnS thin films.

Fig. 10. $(n^2 - 1)^{-1}$ versus $(\lambda)^{-2}$ of γ-MnS thin films.

Fig. 11. Absorption spectrum versus film thickness.

Fig. 12. Dependence of Photocurrent density with thickness

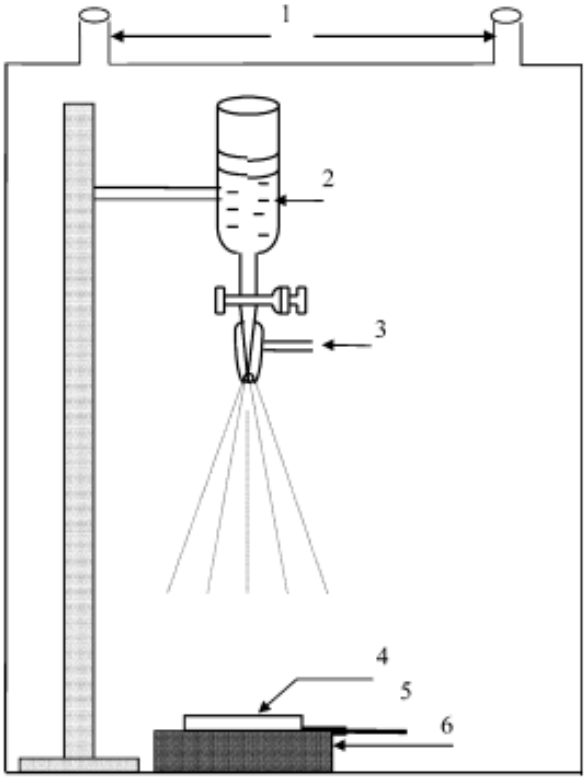

Fig. 1. Schematic diagram of the spraying pyrolysis process: (1) Aspiration system (2) spraying solution (3) carrier gas (4) glass substrates (5) thermocouple (6) hot plate.

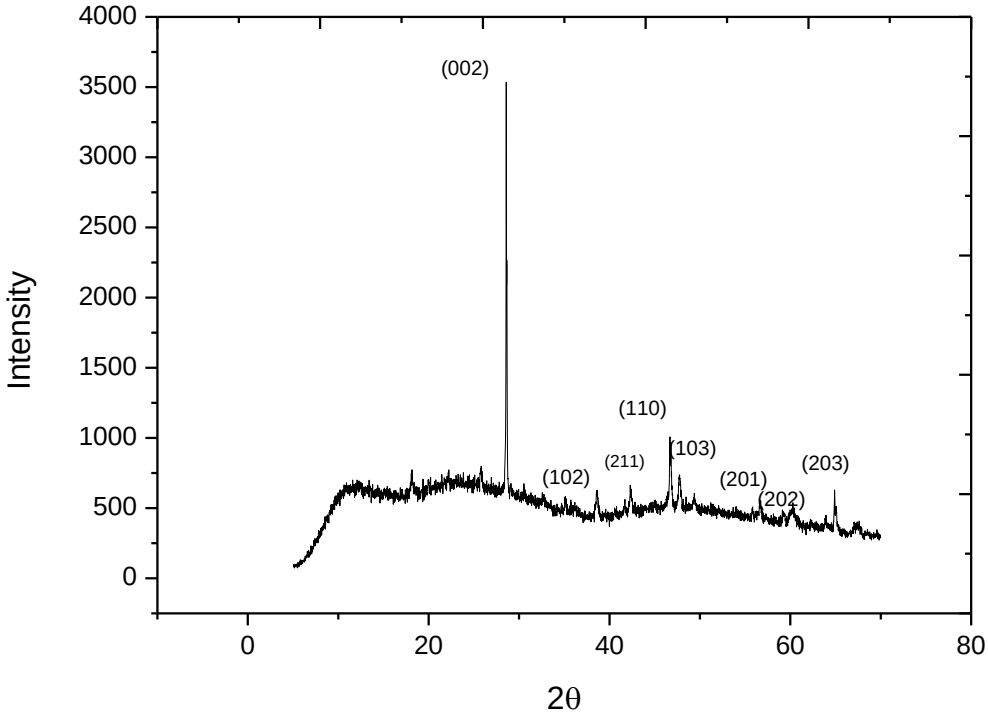

Fig. 2. XRD patterns of γ-MnS thin film.

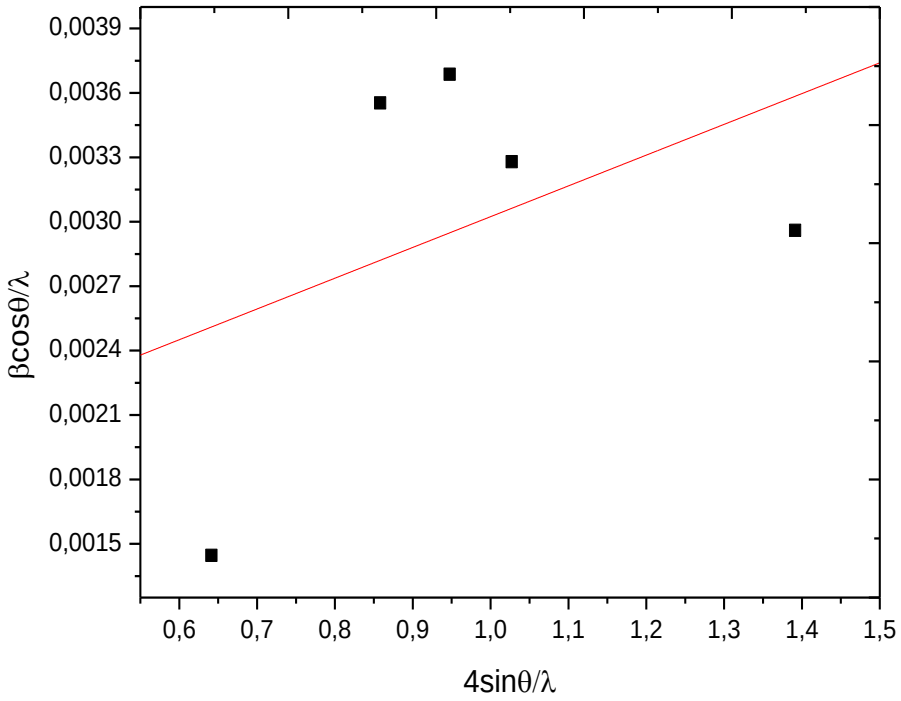

Fig. 3. Williamson-Hall plot of γ-MnS thin film.

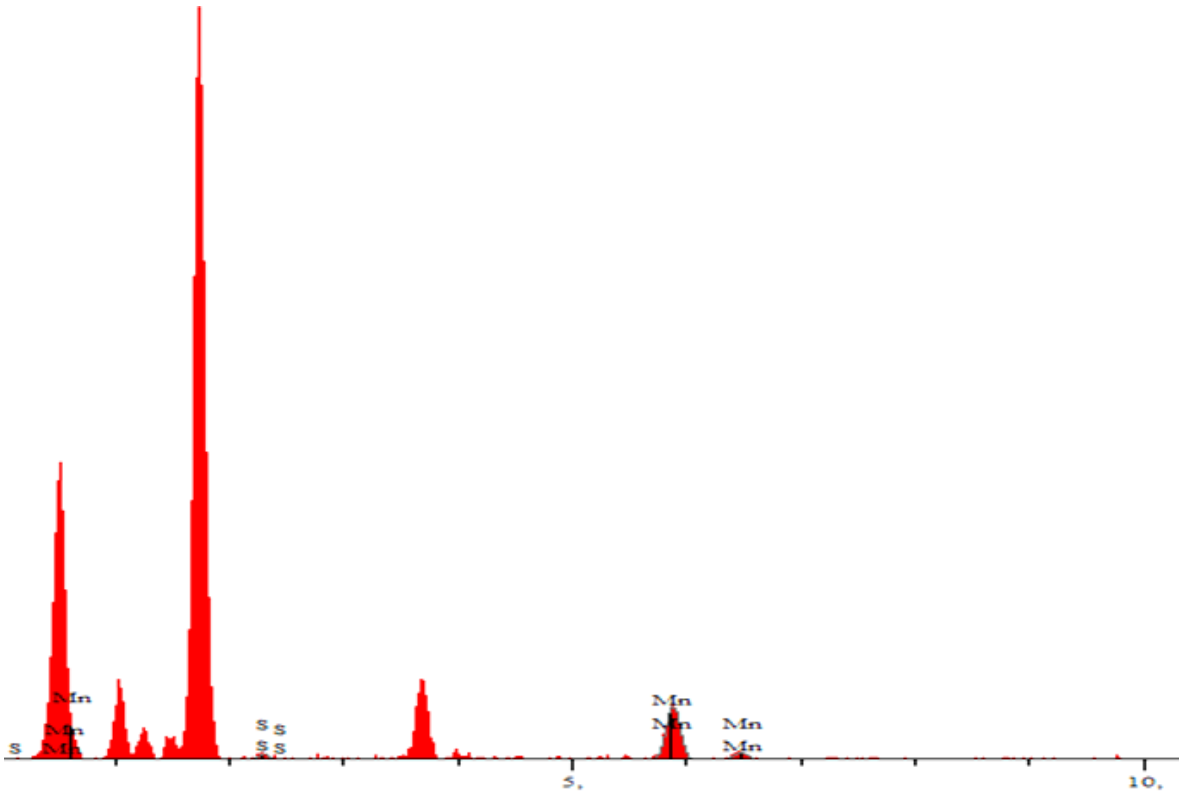

Fig. 4. EDX analysis of γ-MnS thin film.

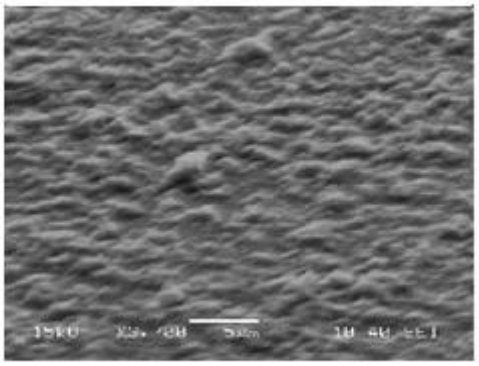

Fig. 5. SEM image of γ-MnS thin film.

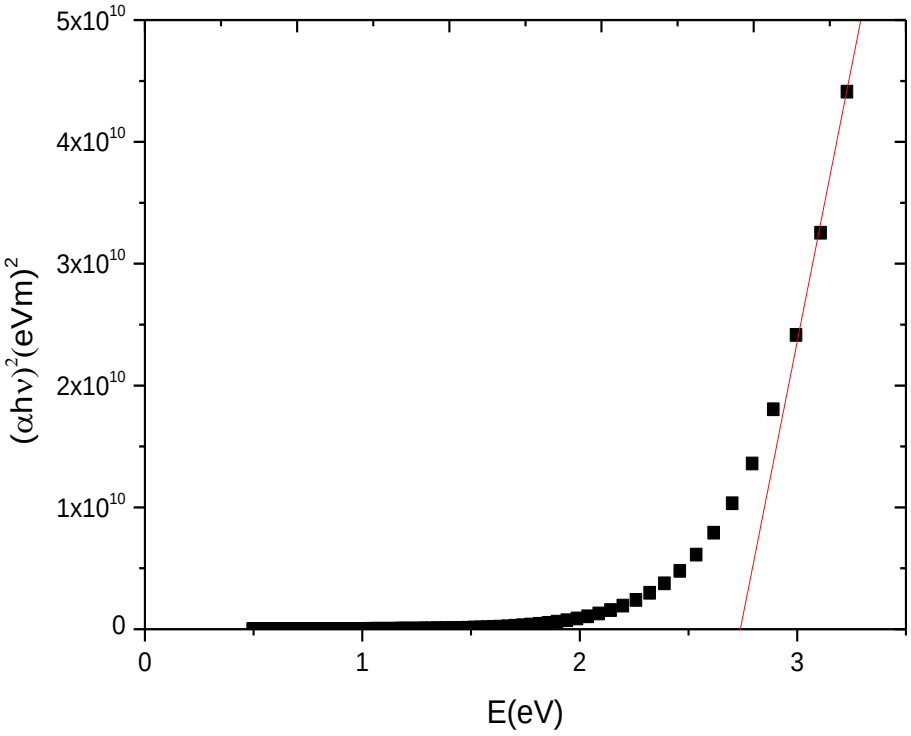

Fig. 6. $(\alpha h\upsilon)^2$ versus energy of γ-MnS thin films.

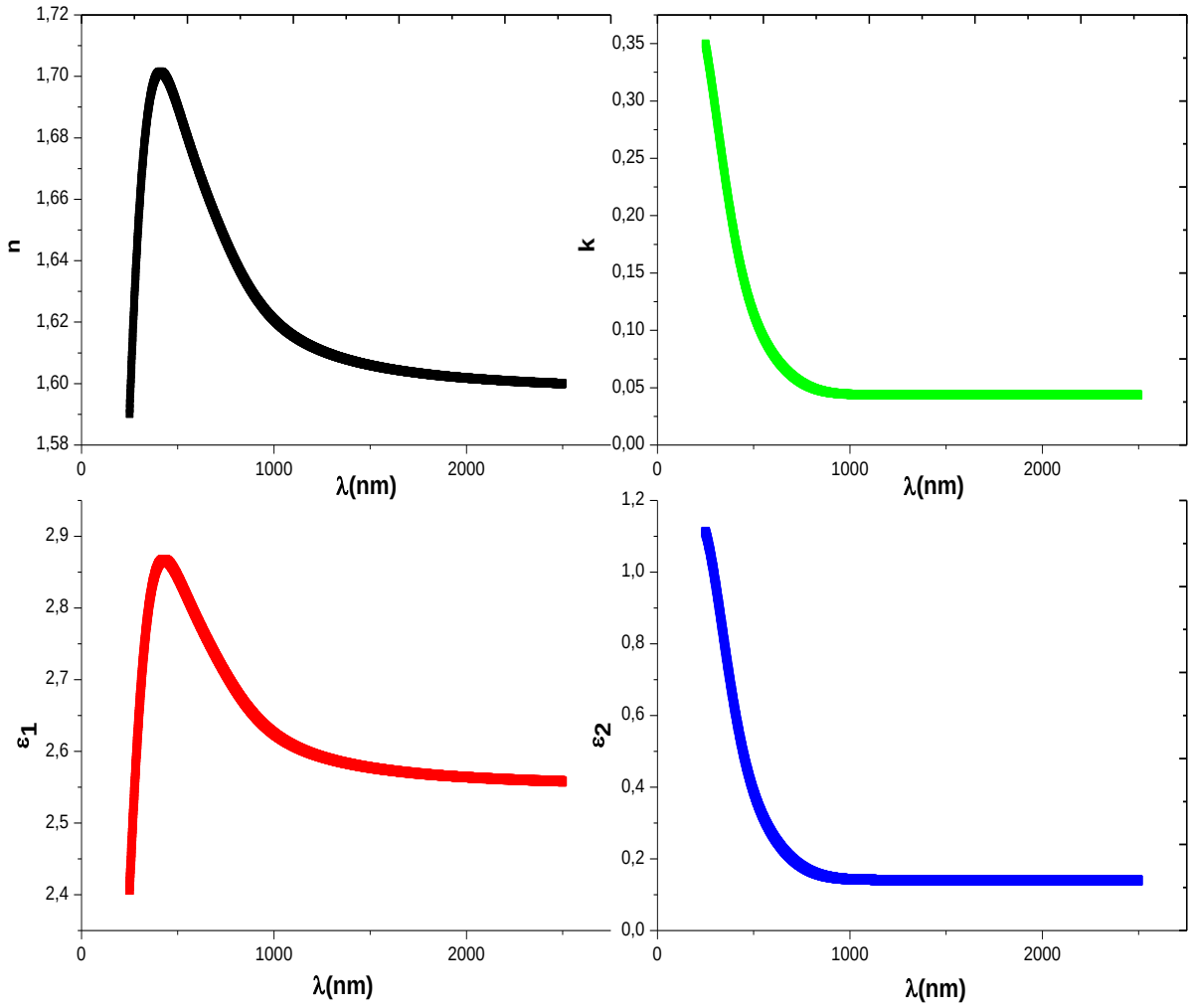

Fig. 7. Optical constants (n, k, ε_1, ε_2) versus energy wavelength of γ-MnS thin films.

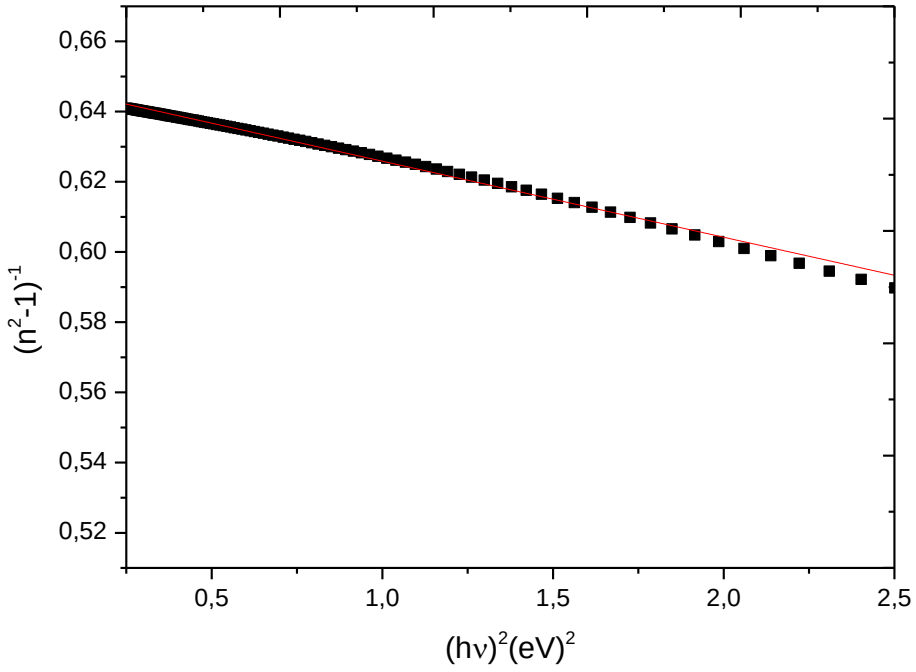

Fig. 8. $(n^2 - 1)$ versus $(h\upsilon)^2$ of γ-MnS thin films.

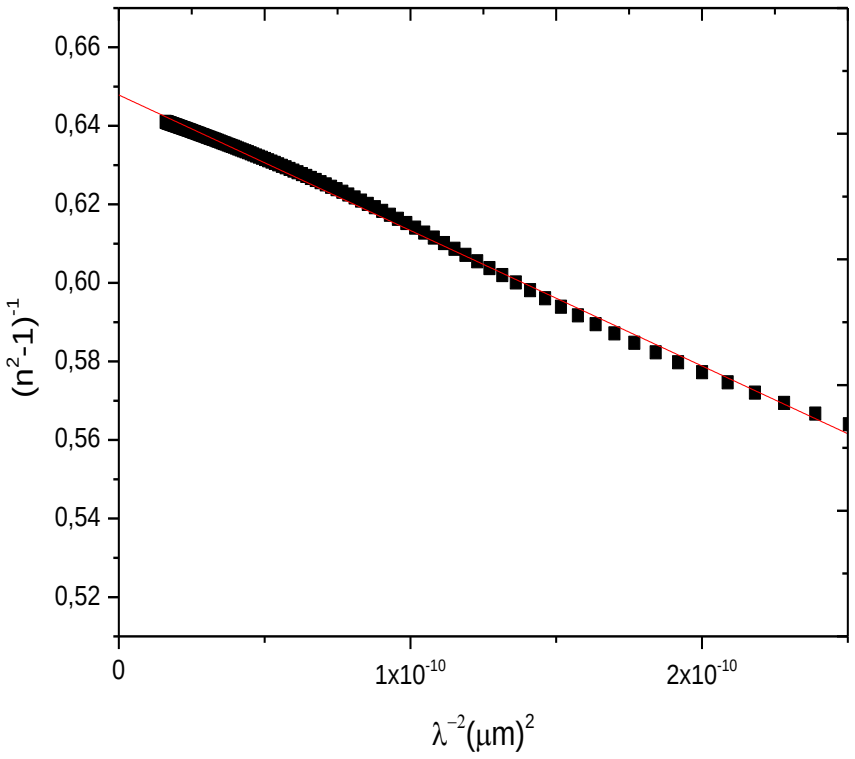

Fig. 9. $(n^2 - 1)^{-1}$ versus $(\lambda)^{-2}$ of γ-MnS thin films.

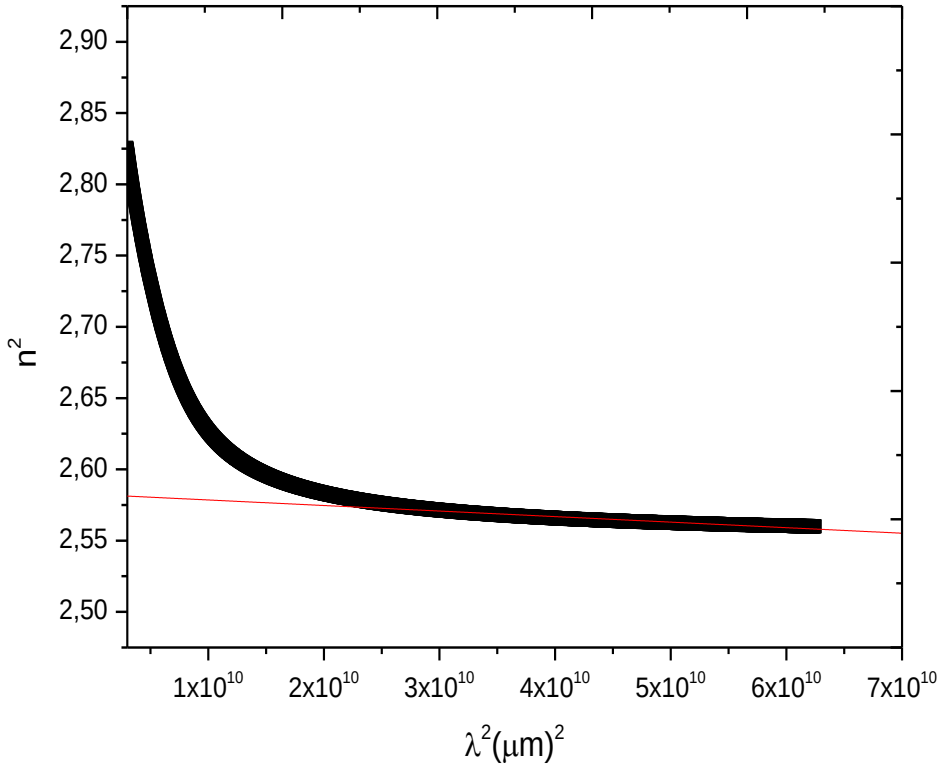

Fig. 10. n^2 versus λ^2 of of γ-MnS thin films.

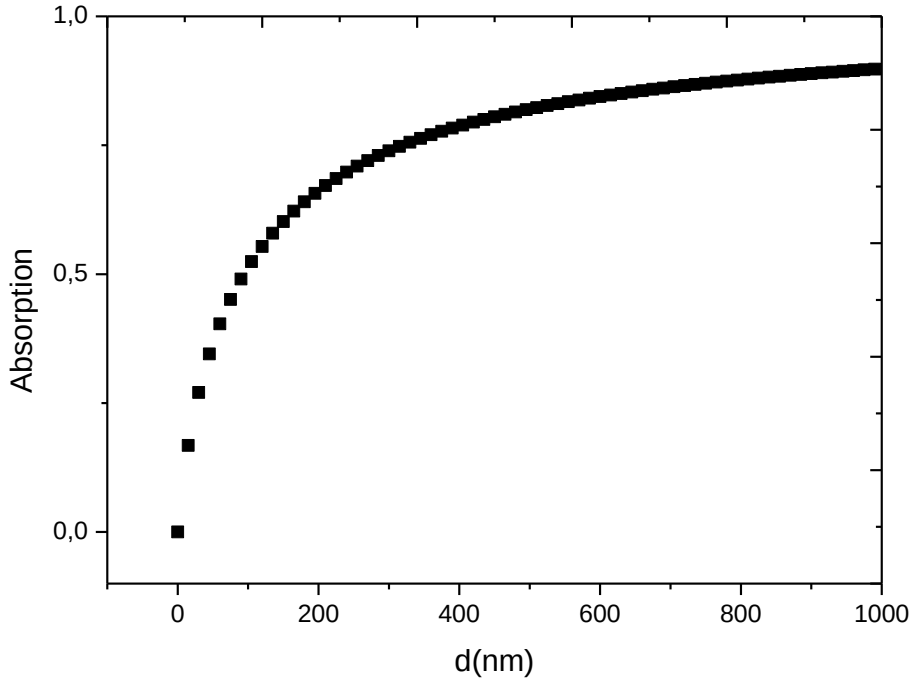

Fig. 11. Absorption spectrum versus film thickness.

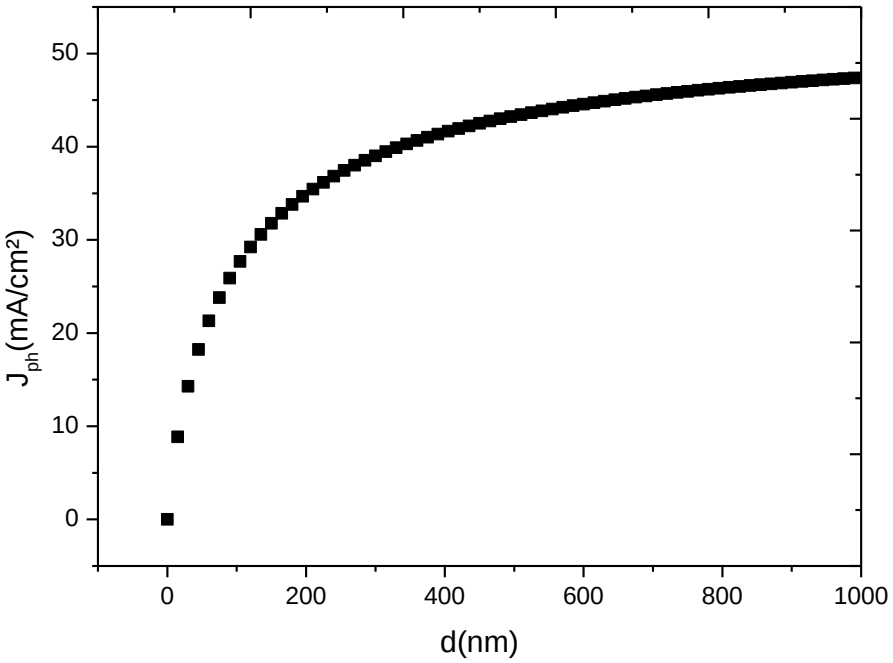

Fig. 12. Dependence of Photocurrent density with thickness

Table list:

Table. 1. Values of optical constants of γ-MnS thin film.

Table. 2. Values of optical constants of γ-MnS thin film.

Table. 3. Values of Hall Effect measurement of γ-MnS thin film.

Elements	**Wt %**	**At %**
Mn (K line)	94.84	91.5
S (K line)	5.15	8.5

Table. 1. EDX elemental analysis of γ-MnS thin film.

Eg(eV)	E_d(eV)	E_0(eV)	M_{-1}	M_{-3}(eV)$^{-2}$	Thickness
	8.83	5.65	1.56	0.0048	303. nm

Table. 2. Values of optical constants of γ-MnS thin film.

ε_L	n_∞	λ_0(nm)	ε_∞	$\frac{N}{m^*}$($m^{-3}.kg^{-1}$)
2.584	1.24	282	1.56	1.4E39

Table. 3. Values of optical constants of γ-MnS thin film.

Resistivity ρ (Ωcm)	Bulk concentration (cm^{-3})	Mobility μ (cm^2/V.S)	Hall Coefficient (cm^2/C)
1150	1.68^e14	32,1	3.7e4

Table. 4. Values of Hall Effect measurement of γ-MnS thin film.